Available online at www.sciencedirect.com
SCIENCE DIRECT®
International Journal of Heat and Mass Transfer 49 (2006) 1480–1488
International Journal of HEAT and MASS TRANSFER
www.elsevier.com/locate/ijhmt

Modeling two-dimensional diffusion-controlled wet chemical etching using a total concentration approach

P. Rath [a], J.C. Chai [a,*], H. Zheng [b], Y.C. Lam [a], V.M. Murukeshan [a]

[a] School of Mechanical and Aerospace Engineering, Nanyang Technological University, 50 Nanyang Avenue, Singapore 639798, Singapore
[b] Singapore Institute of Manufacturing Technology, Singapore 638075, Singapore

Received 2 February 2005; received in revised form 6 September 2005
Available online 22 November 2005

Abstract

A total concentration fixed-grid approach analogous to the enthalpy method for melting/solidification is presented in this article to model two-dimensional diffusion-controlled wet chemical etching. A total concentration, which is the sum of the unreacted and the reacted concentrations is defined. Using this newly defined total concentration, the governing equation also contains the interface condition. For demonstration purposes, the finite-volume method is used to solve the resulting set of governing equation, initial condition and boundary conditions. The results obtained using the total concentration method are compared with solutions from the asymptotic solution and the finite element method. The effects of mask thickness and initial concentration on evolution of etchfront during etching are examined. High initial etchant concentration leads to faster etching and hence the speed of etchfront. It is seen that when mask thickness increases, the bulging effect near the mask corner is less pronounced.

1. Introduction

Wet chemical etching (WCE) is a technique which removes material selectively from the surface of a solid body commonly referred to as the substrate. This is achieved by the application of fluids called etchant to give a specific pattern on the surface of the substrate. WCE process is used in the manufacturing of shadow mask for color-television tubes [1], IC devices in microelectronics industries [2], MEMS devices such as hinges [3] and pressure sensors [4] etc.

The asymptotic solution [5,6], the variational inequality approach [7,8], the moving-grid (MG) approach [7,9,11–14], the level-set method [15–17], and the fixed-grid (FG) method [18,19] have been used to model WCE. Based on the rate of reaction, two possible cases namely—the diffusion-controlled [5–12,18,19] and the reaction-controlled [7,11–14,19] etching are examined by various researchers. These two cases are studied in the modeling of one-dimensional [9,13,18,19] and two-dimensional [5–12,15,17] WCE using the above analytical and numerical approaches. The forced and natural convection effects on etching process are studied by Shin and Economou [11,12].

Two-dimensional WCE is modeled by Kuiken [5,6] using asymptotic solution. The asymptotic solution is valid for diffusion-controlled etching using a dilute etchant. Kuiken et al. [9] presented the exact solution for the diffusion-controlled WCE in a one-dimensional geometry. The analytical treatment is then extended to a two-dimensional diffusion-controlled WCE based on perturbation principle. The substrate is partly protected by a semi-infinite mask (infinitely thin) making it a two-dimensional etching problem. The analytical asymptotic solution is verified with the experimental results for etching GaAs in $HCl/H_2O_2/H_2O$ etchant solution [10].

The MG method has been used to model WCE process. In the MG method, since the computational domain is limited to the space occupied by the etchant, it continuously expands with time. The etchant concentration is solved using appropriate boundary conditions and a specified

* Corresponding author. Tel.: +65 6790 4270; fax: +65 6792 4062.
E-mail address: mckchai@ntu.edu.sg (J.C. Chai).

0017-9310/$ - see front matter © 2005 Elsevier Ltd. All rights reserved.
doi:10.1016/j.ijheatmasstransfer.2005.09.021

Nomenclature

a	coefficient of the discretization equation
c	unreacted etchant concentration
c_R	reacted etchant concentration
$c_{R,max}$	maximum possible value of the reacted concentration
c_T	total concentration
D	diffusion coefficient of etchant
M_{Sub}	molecular weight of the substrate
m	stoichiometric reaction parameter
t	time
t^*	non-dimensional time
$v_{\hat{n}}$	normal speed of the etchant–substrate interface
x, y	coordinate directions
X, Y	non-dimensional coordinate directions

Greek symbols

α	under-relaxation factor
β	non-dimensional etching parameter
∇	vector differential operator
Δt	time step
ρ_{Sub}	density of the substrate

Subscripts

0	initial
P	control volume P
Sub	the substrate
Et	the etchant
T	total

Superscripts

m	iteration number
o	previous time step

initial condition. Using the interface condition at the etchant–substrate interface, the etchfront velocities are then calculated to find the new position of the interface. The process is repeated until the desired etch depth has been achieved or when the specified etching time has been reached. As the computational domain expands with time, the computation mesh has to be regenerated at every time step. Due to the movement of the mesh, a diffusion problem becomes a convective–diffusion problem. The mesh velocities are accounted for in the governing equation in terms of an extra convective term [7,14]. Further, an unstructured mesh system or a body-fitted grid system is needed to model multidimensional WCE.

The numerical models of two-dimensional WCE are presented by Vuik and Cuvelier [7]. The finite element method (FEM) is used for discretization of the problem in the space variables and a finite difference method is used for discretizing the time variable. The MG method and the variational inequality approach are used to track the etchant–substrate interface. The mesh velocities in the MG method due to the movements of the computational grids are modeled. Bruch et al. [8] developed a highly efficient parallel algorithm based on the variational inequality approach for the same etching problem. Shin and Economou [11] studied the effect of etchant flow field (forced convection) on the shape evolution of etching cavities. The FEM was used to solve for the etchant velocity distribution and the etchant concentration distribution in the etched cavities. The MG method was used to track the etchant–substrate interface. The extra convective term due to grid velocities was neglected. The FEM model is extended to compare the effects of forced and natural convection on the shape evolution of etching cavities [12]. Li et al. [13] presented a one-dimensional moving boundary numerical scheme to predict the motion of the etchant–substrate interface during etching of phosphosilicate-glass (PSG) with hydrofluoric acid (HF). In the model a one-dimensional radial diffusion equation is solved using fully implicit scheme. Kaneko et al. [14] used a MG approach to model a two-dimensional reaction-controlled WCE of an aluminium substrate using the FEM. A first order reaction kinetic was assumed. The extra convective term due to grid velocities was also taken into account. Adalsteinsson and Sethian [15,16] developed a level-set formulation to simulate deposition, etching, and lithography in integrated circuit fabrication using two-dimensional and three-dimensional models. La Magna et al. [17] used a level-set method for a moving front to simulate two-dimensional profile evolution during the reaction-controlled WCE process.

Chai and co-workers [18,19] presented a fixed-grid approach based on the total concentration of etchant to model WCE process. This method is analogous to the enthalpy method used in the modeling of melting/solidification process [20–29]. A total concentration, which is the sum of the unreacted etchant concentration and the reacted etchant concentration is defined. The governing equation based on the total concentration includes the interface condition. Hence there is no necessity to compute the etchfront explicitly unlike the MG approaches. In this formulation, the reacted concentration of the etchant is a measure of the etchfront profile during the etching process. Unlike the MG method, the etchfront is found implicitly with the total concentration method. Since the grids are fixed, there is no grid velocity. Hence a diffusion problem always remains a diffusion problem. Cartesian grid can be used to capture the complicated etchfront evolution in multidimensional etching. The model has been tested for

one-dimensional diffusion-controlled [18] and reaction-controlled [19] WCE.

In this article, the fixed-grid (FG) method is extended to model two-dimensional diffusion-controlled WCE. The effect of mask thickness on mask undercutting is examined. The effect of initial etchant concentration on etch profile evolution is also examined.

The remainder of this article is divided into six sections. In the next section, a two-dimensional WCE problem, the governing equation, the interface condition and the boundary conditions are described. Various ingredients of the proposed FG method are then discussed. A brief description of the numerical method used in this article is given. The overall solution procedure is then summarized. Discussions of the results obtained using the proposed FG method is presented. Some concluding remarks are then given.

2. Problem description and governing equations

The schematic and computational domain for the two-dimensional problem considered is shown in Fig. 1. A gap of $2a$ is to be etched in a substrate (Fig. 1a). For demonstration purposes, the width of the mask on both sides of the gap is assumed to be large enough so that the concentration of etchant far away from the gap will remain unaltered at the initial concentration. The initial concentration of the etchant at $t = 0$ is c_0. At $t > 0$, the reaction between the etchant and the substrate at the etchant–substrate interface results in the reduction of the concentration of etchant adjacent to the etchant–substrate interface and the depletion of the substrate. The concentration of etchant on the boundaries far away from the gap is kept at the initial concentration, i.e. $c = c_0$. The etching is assumed diffusion-controlled where reaction rate is infinitely fast. The origin of the coordinate system is set to the etchant–substrate interface at the center of the gap. Since the problem is symmetrical about the origin, only half of the domain is considered as shown in Fig. 1b. The governing equation, the interface condition and the boundary conditions are presented next.

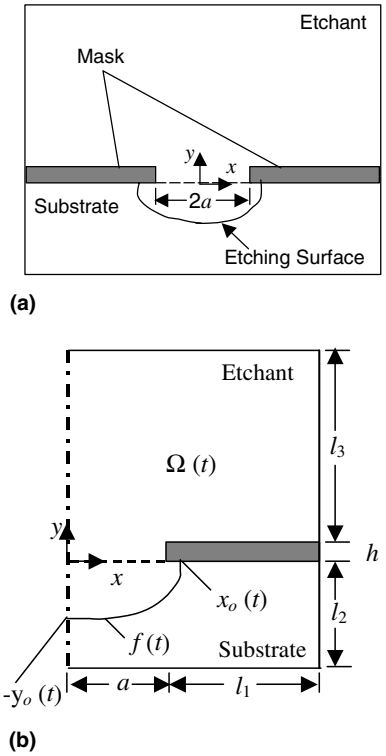

Fig. 1. Schematic of the two-dimensional etching problem: (a) a full schematic, (b) the computational domain.

2.1. Governing equation

For a stationary etchant solution, the etchant concentration within the etchant domain is governed by the mass diffusion equation given by

$$\frac{\partial c}{\partial t} = \frac{\partial}{\partial x}\left(D\frac{\partial c}{\partial x}\right) + \frac{\partial}{\partial y}\left(D\frac{\partial c}{\partial y}\right) \quad \text{in } \Omega(t) \tag{1a}$$

The initial and boundary conditions are

Initial condition at $t = 0$

$$c = c_0 \quad \text{in } \Omega(t) \tag{1b}$$

Boundary conditions for $t > 0$

$$\frac{\partial c}{\partial x} = 0 \quad x = 0 \tag{1c}$$

$$c = c_0 \quad y = h + l_3 \tag{1d}$$

$$c = c_0 \quad x = a + l_1,\ h \leqslant y \leqslant h + l_3 \tag{1e}$$

$$J_y = -D\frac{\partial c}{\partial y} = 0 \quad y = h,\ a \leqslant x \leqslant a + l_1 \text{ and } y = 0,\ a \leqslant x \leqslant a + x_0(t) \tag{1f}$$

$$J_x = -D\frac{\partial c}{\partial x} = 0 \quad x = a,\ 0 \leqslant y \leqslant h \tag{1g}$$

$$c = 0 \quad \text{in the substrate and etchant–substrate interface} \tag{1h}$$

Interface condition for $t > 0$ on $f(t)$

$$\vec{v} = -\frac{DM_{\text{Sub}}}{m\rho_{\text{Sub}}}\nabla c \tag{1i}$$

where $\vec{v}$ is the velocity of the etchant–substrate interface, D is the diffusion coefficient of etchant, M_{Sub} is the molecular weight of the substrate, ρ_{Sub} is the density of the substrate and m is the stoichiometric reaction parameter of the etchant–substrate reaction. The normal speed of the etchant–substrate interface $v_{\hat{n}}$ is obtained by dotting both sides of Eq. (1i) with the unit vector $\hat{n}$ normal to the interface which points towards the substrate region. This can be written as

$$\vec{v}\cdot\hat{n} = -\frac{DM_{\text{Sub}}}{m\rho_{\text{Sub}}}\nabla c\cdot\hat{n} \Rightarrow v_{\hat{n}} = -\frac{DM_{\text{Sub}}}{m\rho_{\text{Sub}}}\frac{\partial c}{\partial \hat{n}} \tag{1j}$$

3. The total concentration method

In this article the *total concentration* of the etchant is defined as

$$c_T \equiv c + c_R \tag{2}$$

where c_T is the total concentration, c is the unreacted etchant concentration and c_R is the reacted etchant concentration, respectively. Physically, c_R is the etchant concentration *consumed* in the reaction process. As such it is constant except at the etchant–substrate interface. This is used to capture the etchfront implicitly. The value of c_R changes from 0 to its maximum possible value of $c_{R,max}$ in a control volume where etching is taking place. The maximum possible value of the reacted concentration termed $c_{R,max}$, is the amount of etchant required per unit volume of substrate to dissolve the substrate during reaction. In a unit volume, there are ρ_{Sub}/M_{Sub} moles of substrate. The reaction between the etchant and the substrate is given as

$$S + mE \rightarrow qP \tag{3}$$

where S is the substrate, E is the etchant and P is the product respectively. From Eq. (3) it is seen that the amount of etchant needed to dissolve a unit volume of substrate is $m\rho_{Sub}/M_{Sub}$. As $c_{R,max}$ is the amount of etchant required per unit volume of substrate to dissolve the substrate during reaction, it can be written as

$$c_{R,max} = \frac{m\rho_{Sub}}{M_{Sub}} \tag{4}$$

The governing equation based on the total concentration is given by

$$\frac{\partial c_T}{\partial t} = \frac{\partial}{\partial x}\left(D\frac{\partial c}{\partial x}\right) + \frac{\partial}{\partial y}\left(D\frac{\partial c}{\partial y}\right) \tag{5}$$

Using Eq. (2), Eq. (5) can be written as

$$\frac{\partial c}{\partial t} = \frac{\partial}{\partial x}\left(D\frac{\partial c}{\partial x}\right) + \frac{\partial}{\partial y}\left(D\frac{\partial c}{\partial y}\right) - \frac{\partial c_R}{\partial t} \tag{6}$$

This equation is valid in both the etchant and the substrate regions. The interface condition given by Eq. (1j) is contained in Eq. (6) implicitly. This is shown next.

3.1. Interface condition

The integral form of the governing equation (Eq. (5)) based on the total concentration is given as

$$\int_A \nabla c \cdot \hat{n}\,dA = \frac{d}{dt}\int_V c_T\,dV \tag{7}$$

where A is the surface area and $\hat{n}$ is outward normal on the surface A. Consider an elementary control volume V (which contains the interface) as shown in Fig. 2 at two time intervals. At $t + \Delta t$, ΔV volume of the substrate is etched away from the elementary control volume V. At

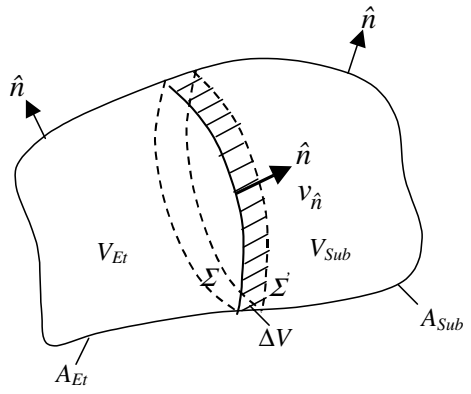

Fig. 2. A control volume containing the etchant–substrate interface.

time t, the interfacial surface Σ divides the control volume V into a etchant portion V_{Et} and a substrate portion V_{Sub} and divides the surface area A of V into two parts namely, A_{Et} and A_{Sub}. After a small increment in time Δt, the interface occupies a new position Σ' and during this time ΔV volume of substrate has been etched away. Now the integral on the right hand side of Eq. (7) is examined at time t and $t + \Delta t$. At time t,

$$\int_V c_T^t\,dV = \int_{V_{Et}} \left(c_T^t\right)_{Et} dV + \int_{V_{Sub}-\Delta V} \left(c_T^t\right)_{Sub} dV + \int_{\Delta V} \left(c_T^t\right)_{Sub} dV \tag{8}$$

where the subscripts Et and Sub represent the etchant and the substrate respectively. At time $t + \Delta t$,

$$\int_V c_T^{t+\Delta t}\,dV = \int_{V_{Et}} \left(c_T^{t+\Delta t}\right)_{Et} dV + \int_{V_{Sub}-\Delta V} \left(c_T^{t+\Delta t}\right)_{Sub} dV + \int_{\Delta V} \left(c_T^{t+\Delta t}\right)_{Et} dV \tag{9}$$

Subtracting Eq. (8) from Eq. (9), gives

$$\int_V \left(c_T^{t+\Delta t} - c_T^t\right) dV = \int_{V_{Et}} \left(c_T^{t+\Delta t} - c_T^t\right)_{Et} dV + \int_{V_{Sub}-\Delta V} \left(c_T^{t+\Delta t} - c_T^t\right)_{Sub} dV + \int_{\Delta V} \left[\left(c_T^{t+\Delta t}\right)_{Et} - \left(c_T^t\right)_{Sub}\right] dV \tag{10}$$

Dividing both sides of Eq. (10) by Δt, and taking limits as Δt approaches zero. It should be noted that as $\Delta t \rightarrow 0$, $(V_{Sub} - \Delta V) \rightarrow V_{Sub}$. Hence Eq. (10) reduces to

$$\frac{d}{dt}\int_V c_T\,dV = \frac{d}{dt}\int_{V_{Et}} (c_T)_{Et}\,dV + \frac{d}{dt}\int_{V_{Sub}} (c_T)_{Sub}\,dV + \lim_{\Delta t \rightarrow 0}\int_{\Delta V} \frac{\left[\left(c_T^{t+\Delta t}\right)_{Et} - \left(c_T^t\right)_{Sub}\right]}{\Delta t}\,dV \tag{11}$$

Using Eq. (7), the integrals over V_{Et} and V_{Sub} can be replaced as

$$\frac{\mathrm{d}}{\mathrm{d}t}\int_V c_\mathrm{T}\,\mathrm{d}V = \int_{A_{\mathrm{Et}}+\Sigma}(\nabla c)_{\mathrm{Et}}\cdot\hat{n}\,\mathrm{d}A + \int_{A_{\mathrm{Sub}}+\Sigma}(\nabla c)_{\mathrm{Sub}}\cdot\hat{n}\,\mathrm{d}A + \lim_{\Delta t\to 0}\int_{\Delta V}\frac{\left[\left(c_\mathrm{T}^{t+\Delta t}\right)_{\mathrm{Et}} - \left(c_\mathrm{T}^{t}\right)_{\mathrm{Sub}}\right]}{\Delta t}\,\mathrm{d}V \tag{12}$$

Now considering the last term of Eq. (12), at time t the interface is occupied by the substrate. As the interface is occupied by the substrate, the reacted concentration is zero. Therefore,

$$\left(c_\mathrm{T}^{t}\right)_{\mathrm{Sub}} = c^{t} + c_\mathrm{R}^{t} = c^{t} \tag{13}$$

At time $t+\Delta t$, the total concentration is

$$\left(c_\mathrm{T}^{t+\Delta t}\right)_{\mathrm{Et}} = c^{t+\Delta t} + c_\mathrm{R}^{t+\Delta t} \tag{14}$$

As $\Delta t \to 0$, the unreacted etchant concentration $c^{t+\Delta t} \to c^{t}$ and the reacted concentration $c_\mathrm{R}^{t+\Delta t} \to c_{\mathrm{R,max}}$. Again as $\Delta t \to 0$, the ratio $\mathrm{d}V/\Delta t$ approaches $v_{\hat{n}}\,\mathrm{d}\Sigma$, where $v_{\hat{n}}$ is the local normal speed of the interfacial surface element $\mathrm{d}\Sigma$ towards the substrate region. Also, the space that is enclosed by ΔV shrinks to the surface Σ, so that the region of integration becomes Σ. If $\hat{n}$ represents the local outward normal to Σ towards the substrate region, then for a portion of the integrals over Σ, $\hat{n} = \hat{n}$ and $\hat{n} = -\hat{n}$ for the etchant and the substrate side respectively. As a result, Eq. (12) reduces to

$$\frac{\mathrm{d}}{\mathrm{d}t}\int_V c_\mathrm{T}\,\mathrm{d}V = \int_A \nabla c\cdot\hat{n}\,\mathrm{d}A + \int_\Sigma\left[\left(\frac{\partial c}{\partial \hat{n}}\right)_{\mathrm{Et}} - \left(\frac{\partial c}{\partial \hat{n}}\right)_{\mathrm{Sub}}\right]\mathrm{d}\Sigma + \int_\Sigma c_{\mathrm{R,max}} v_{\hat{n}}\,\mathrm{d}\Sigma \tag{15}$$

Using Eq. (7), Eq. (15) reduces to

$$\int_\Sigma\left[\left(\frac{\partial c}{\partial \hat{n}}\right)_{\mathrm{Et}} - \left(\frac{\partial c}{\partial \hat{n}}\right)_{\mathrm{Sub}} + c_{\mathrm{R,max}} v_{\hat{n}}\right]\mathrm{d}\Sigma = 0$$

$$\Rightarrow \left(\frac{\partial c}{\partial \hat{n}}\right)_{\mathrm{Et}} - \left(\frac{\partial c}{\partial \hat{n}}\right)_{\mathrm{Sub}} + c_{\mathrm{R,max}} v_{\hat{n}} = 0 \tag{16}$$

In the substrate, the etchant concentration is zero. As a result, the second term of Eq. (16) will be zero. Hence Eq. (16) reduces to

$$\frac{\partial c}{\partial \hat{n}} = -c_{\mathrm{R,max}} v_{\hat{n}} \tag{17}$$

Substituting $c_{\mathrm{R,max}}$ from Eq. (4) in the above equation and rearranging results in

$$v_{\hat{n}} = -\frac{DM_{\mathrm{Sub}}}{m\rho_{\mathrm{Sub}}}\frac{\partial c}{\partial \hat{n}}$$

Above relation is the interface condition given in Eq. (1j). A procedure to update the reacted concentration (c_R) is needed to complete the formulation. This is discussed next.

3.2. Procedure to update c_R

A procedure to calculate the reacted etchant concentration c_R is presented in this section. As the reacted concentration is constant away from the etchant–substrate interface, Eq. (6) reduces to the original governing equation (Eq. (1a)) except at the etchant–substrate interface. At the etchant–substrate interface, the reacted etchant concentration is a measure of the amount of substrate being etched. In the proposed FG method, the control volumes where etching is taking place (see Fig. 3) are identified and are called the etching-control-volume (ECV). The ECVs are the substrate control volumes adjacent to the etchant control volumes. In an ECV, c_R changes from 0 to its maximum possible value of $c_{\mathrm{R,max}}$. A procedure to update c_R in the ECV is described in this section. The finite volume discretization equation (using the fully implicit scheme) of Eq. (6) for an ECV (control volume P) is given as

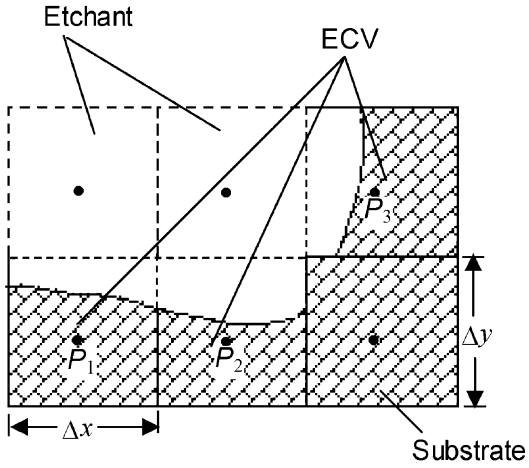

Fig. 3. Control volumes P_1, P_2, P_3 undergoing etching.

$$a_P c_P^{m} = \sum a_{\mathrm{nb}} c_{\mathrm{nb}}^{m} + a_P^{\mathrm{o}} c_P^{\mathrm{o}} - \left(c_{\mathrm{R},P}^{m} - c_{\mathrm{R},P}^{\mathrm{o}}\right)\frac{\Delta V_P}{\Delta t} \tag{18}$$

where m is the mth iteration of the current time step, o is the previous time step, P is the control volume P, nb is the neighboring control volumes, a is the coefficients of the discretization equation, ΔV is the volume of a control volume and Δt is the time step respectively. Eq. (18) is valid for all control volumes. However, as c_R is constant in the etchant and substrate, the last term on the right side of Eq. (18) is zero except in the ECV. At the $(m+1)$th iteration, Eq. (18) can be written as

$$a_P c_P^{m+1} = \sum a_{\mathrm{nb}} c_{\mathrm{nb}}^{m+1} + a_P^{\mathrm{o}} c_P^{\mathrm{o}} - \left(c_{\mathrm{R},P}^{m+1} - c_{\mathrm{R},P}^{\mathrm{o}}\right)\frac{\Delta V_P}{\Delta t} \tag{19}$$

Subtracting Eq. (19) from Eq. (18) and rearranging, gives

$$c_{\mathrm{R},P}^{m+1} = c_{\mathrm{R},P}^{m} + \frac{\Delta t}{\Delta V_P}\left[a_P\left(c_P^{m} - c_P^{m+1}\right) + \sum a_{\mathrm{nb}}\left(c_{\mathrm{nb}}^{m+1} - c_{\mathrm{nb}}^{m}\right)\right] \tag{20}$$

When the solution converges, the last term of Eq. (20) will be zero. However, during the initial iteration process, it is most likely a non-zero term. Realizing that it is zero upon convergence, this term can be ignored from the calculation and Eq. (20) becomes

$$c_{\mathrm{R},P}^{m+1} = c_{\mathrm{R},P}^{m} + \alpha a_P \frac{\Delta t}{\Delta V_P}(c_P^m - c_P^{m+1}) \tag{21}$$

where α is an under-relaxation factor. For a diffusion-controlled reaction, the reaction rate at the interface is infinitely fast which makes the concentration at the interface zero. For diffusion-controlled reaction, FG procedure ensures that $c_P^{m+1} = 0$ and the excess concentration is used to update the reacted concentration. With $c_P^{m+1} = 0$, Eq. (21) becomes

$$c_{\mathrm{R},P}^{m+1} = c_{\mathrm{R},P}^{m} + \alpha a_P \frac{\Delta t}{\Delta V_P} c_P^m \tag{22}$$

Within the control volume where etching is taking place, the reacted concentration is updated using Eq. (22). Etching for a given control volume completed, when $c_{\mathrm{R},P}^{m+1}$ reaches $c_{\mathrm{R,max}}$.

4. Numerical method

In this article, the finite-volume method (FVM) of Patankar [30] is used to solve the concentration equation. Since a detailed discussion of the FVM is available in Patankar [30], only a brief description of the major features of the FVM used is given here. In the FVM, the domain is divided into a number of control volumes such that there is one control volume surrounding each grid point. The grid point is located in the center of a control volume. The governing equation is integrated over each control volume to derive an algebraic equation containing the grid point values of the dependent variable. The discretization equation then expresses the conservation principle for a finite control volume just as the partial differential equation expresses it for an infinitesimal control volume. The resulting solution implies that the integral conservation of mass is exactly satisfied for any control volume and of course, for the whole domain. The resulting algebraic equations are solved using a line-by-line Tri-Diagonal Matrix Algorithm. In the present study, a solution is deemed converged when the maximum change in the concentration and the maximum change in the reacted concentration between two successive iterations are less than 10^{-11}.

5. Overall solution procedure

The overall solution procedure for the proposed total concentration method can be summarized as follows:

1. Specify the etchant domain, the substrate domain and the mask region. Ensure that the etchant–substrate interface lies on the interface between two control volumes.
2. Set the initial etchant concentration as c_0 in the etchant domain and zero in the substrate domain including the mask region.
3. Initially set c_{R} to 0 in the substrate domain including the mask region and to $c_{\mathrm{R,max}}$ in the etchant domain respectively.
4. Advance the time step to $t + \Delta t$.
5. Identify the etching control volumes (ECVs). These are the substrate control volumes with adjacent etchant control volumes.
6. Use the "internal" boundary condition treatment of Patankar [30] (by setting S_P to a big number) to set the unreacted etchant concentration in the mask and substrate regions to zero.
7. Set S_P in the ECV to zero.
8. Solve Eq. (6) for the unreacted concentration.
9. Update the reacted concentration in the ECVs using Eq. (22).
10. Check for convergence.
    (a) If the solution has converged, then check if the required number of time steps has been reached. If yes, stop. If not, repeat (4)–(10).
    (b) If the solution has not converged, then check the calculated reacted concentration.
    - If $c_{\mathrm{R}} < c_{\mathrm{R,max}}$, repeat (8)–(10).
    - If, $c_{\mathrm{R}} \geqslant c_{\mathrm{R,max}}$ then set $c_{\mathrm{R}} = c_{\mathrm{R,max}}$ and repeat (5)–(10).

6. Results and discussions

The two-dimensional problem shown in Fig. 1 is modeled using the proposed total concentration approach. Due to the symmetry of the problem about the y-axis, only half of the domain is modeled as shown in Fig. 1b. For ease of presentation, the following dimensionless variables are defined.

$$X = x/a \tag{23a}$$

$$Y = y/a \tag{23b}$$

$$C = c/c_0 \tag{23c}$$

$$C_{\mathrm{R}} = c_{\mathrm{R}}/c_0 \tag{23d}$$

$$t^* = tD/a^2 \tag{23e}$$

$$\beta = \frac{m\rho_{\mathrm{Sub}}}{c_0 M_{\mathrm{Sub}}} \tag{23f}$$

The non-dimensional width of the mask is taken as $L_1 = l_1/a = 6.5$ and the dimensionless height of etchant is taken as $L_3 = l_3/a = 6.5$. The width and thickness of the substrate are taken as $L_{\mathrm{Sub}} = 1 + L_1 = 7.5$ and $L_2 = l_2/a = 4.0$ respectively. Results for two mask thicknesses namely, infinitely thin and finite thickness are modeled. For infinitely thin mask, the non-dimensional mask thickness is taken as $H = h/a = 0.005$. Further decrease in mask thickness does not alter the solution. For finite mask thickness, the thickness of the mask is taken as one-fourth of the gap width, i.e. $H = h/a = 0.5$. In Eq. (23f), β is the non-dimensional etching parameter, which is a measure of the etchfront speed for the given substrate to be etched. The speed of the etchfront is inversely proportional to β. The parameter β is also a measure of the initial etchant concentration c_0 for a given substrate to be etched. In general if

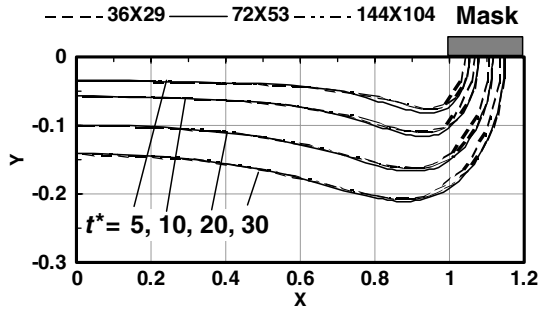

Fig. 4. Grid independent study for $\beta = 100$ and infinitely thin mask.

the initial etchant concentration is higher, the etch rate (the etchfront speed) should be higher. It is clearly evident from the definition of β as it is inversely proportional to the initial etchant concentration. So high initial etchant concentration leads to lower value of β which leads to the faster movement of the etchfront as mentioned above. The detail study of the effect of β on the etchfront movement is discussed later in this article.

A grid refinement study was performed to ensure the solutions are grid (temporal and spatial) independent. Fig. 4 shows the evolution of etch profiles at four different times for $\beta = 100$ and infinitely thin mask. Results from these spatial grid resolutions are shown in Fig. 4. Three control volume sizes are taken to carry out this test. For each control volume size the time independent etch profiles are shown. For the grid sizes of 32×29 and 72×53, the time step size is $\Delta t^* = 0.01$. For the 144×104 grid, the time step size is $\Delta t^* = 0.001$. It is seen that the grid sizes of 72×53 and 144×104 produced the same etch profile for the four given times. As a result, 72×53 control volumes with $\Delta t^* = 0.01$ are used in this article.

Fig. 5a shows the comparisons of etch profiles at different times between the FG method, the asymptotic solution [6] and the MG [11] method. The non-dimensional etching parameter is taken as $\beta = 100$. It is seen from Fig. 5a that the present approach predicts the etch profiles at different times accurately. Some bulging effect is seen near the corner of the mask. The etching is faster near the corner region compared to the region away from the corner. Fig. 5b shows the concentration contours at $t^* = 30$. It is seen that the concentration contours have gone deep into the etched region near the corner of the mask. Hence, the concentration gradient is higher near the mask region. As a result the etching is faster in this region which results in bulging of etch profiles. Fig. 6a shows the comparison of etch profiles for $\beta = 10$. The etch profiles from the present approach compare very well with the variational inequality approach of Bruch et al. [8]. Fig. 6b shows the concentration contour for $\beta = 10$ at $t^* = 20$. It is seen that concentration contours have gone deep at the center of the gap, which results in enlarged bulging region from mask corner to the center compared to the case with $\beta = 100$. This is because of the high initial etchant concentration for $\beta = 10$, which results in faster etch rate. The bulging effect is localized near the

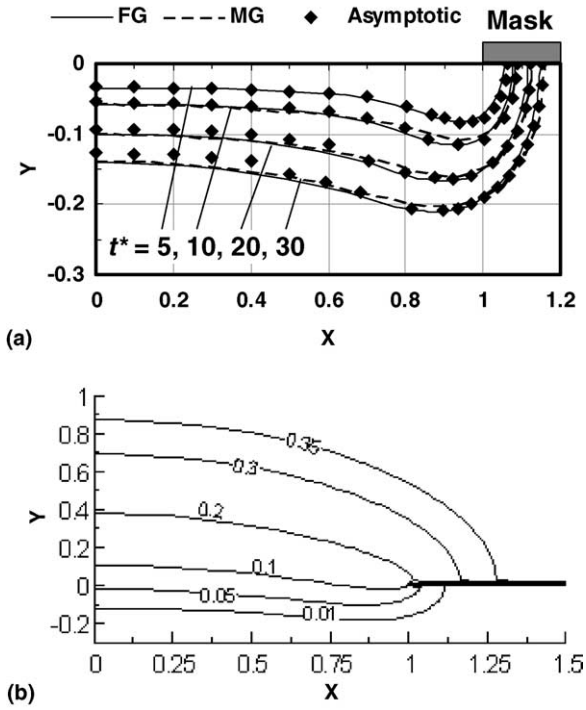

Fig. 5. Etched profiles and concentration distribution for $\beta = 100$ and infinitely thin mask: (a) comparison of etched profiles with existing asymptotic solution and MG method, (b) concentration contours at $t^* = 30$.

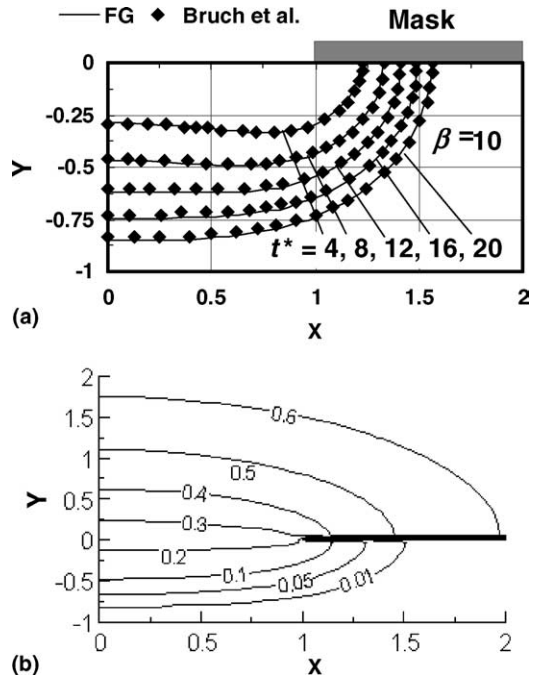

Fig. 6. Etched profiles and concentration distribution for $\beta = 10$ and infinitely thin mask: (a) comparison of etched profiles with the variational inequality approach, (b) concentration contour at $t^* = 20$.

mask corner region only at early time when β decreases to 10 from 100.

Fig. 7a shows the comparisons of the etch profiles evolution for finite mask thickness. The non-dimensional etching parameter is taken as $\beta = 100$. The etch profiles obtained from the present approach compare well with the MG solutions [11]. Fig. 7b shows the concentration contour at $t^* = 126$. It is seen that the concentration contours in the etched region is nearly flat. As a result, the concentration gradient will also be nearly uniform. Hence there is no significant bulging effect seen unlike the case with infinitely thin mask. Fig. 8 shows the etch profiles obtained with both mask thicknesses. It is seen that the bulging effects reduces with mask thickness. It is because of the larger diffusion length of the etchant from the area above the inert mask to the etching surface. Hence fresh etchant is less readily available near the mask corner as thickness of the mask increases which results in slow etch rate near the mask corner.

The effects of the initial etchant concentrations on etch profile evolutions at a given time are shown in Fig. 9. For a given substrate to be etched the initial etchant concentration is varied by varying the non-dimensional etching parameter β (Eq. (23f)). The initial etchant concentration is inversely proportional to β. For this test study, three values of β namely, 1, 10 and 100 are chosen. The mask is taken as infinitely thin. Fig. 9 shows the etch profiles for three β values at $t^* = 20$. It is seen that as β decreases, the initial etchant concentration increases. Therefore the etchdepth increases as β decreases.

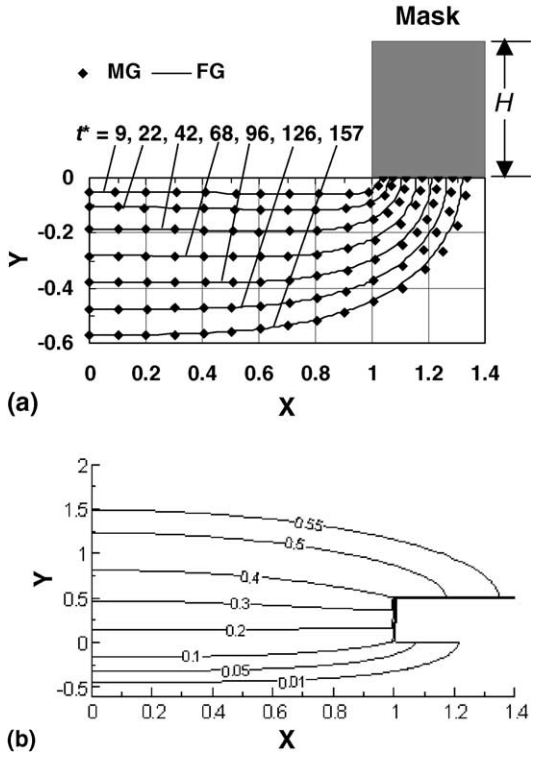

Fig. 7. Etched profiles and concentration distribution for $\beta = 100$ and finite mask thickness ($H = 0.5$): (a) comparison of etched profiles with MG method, (b) concentration contour at $t^* = 126$.

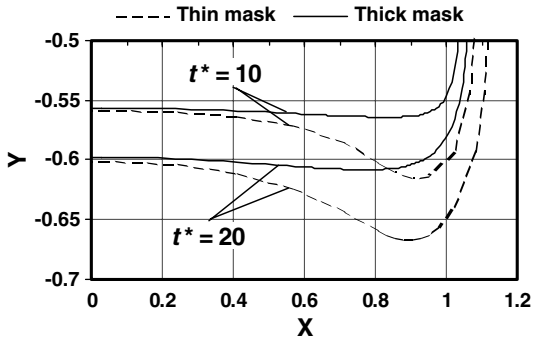

Fig. 8. Effect of mask thickness on bulging of etched profile for $\beta = 100$.

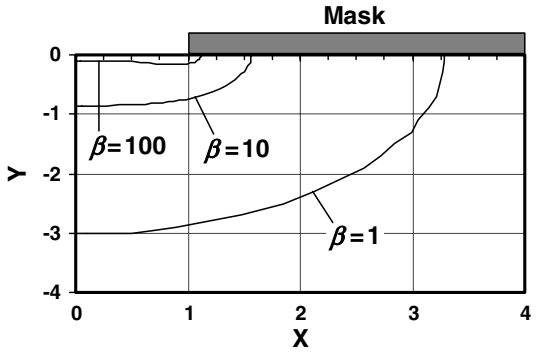

Fig. 9. Effect of initial etchant concentration (in terms of β) on etched profile evolution at $t^* = 20$ for infinitely thin mask.

7. Concluding remarks

A new fixed-grid method based on the total-concentration of etchant has been presented for two-dimensional WCE. The proposed method is analogous to the enthalpy method used in the modeling of melting/solidification processes. A detailed formulation based on the total concentration of the etchant is presented. In the proposed approach the governing equation includes the interface condition. With this proposed method there is no necessity for computing the etchfront position explicitly. The method has been applied to two-dimensional diffusion-controlled etching. For demonstration purposes, the finite-volume method is used to discretize the governing equation. The results from the present approach are compared with the results from other existing methods. The results show that the etchfront profile can be predicted accurately using the proposed method.

References

[1] K.H. Hoffman, J. Sprekels, Free Boundary Problems: Theory and Applications, Longman Scientific and Technical 1 (1990) 89.
[2] M.J. Madou, Fundamentals of Microfabrication, second ed., CRC Press, New York, 2002.
[3] K.S.J. Pister, M.W. Judy, S.R. Burgett, R.S. Fearing, Microfabricated hinges, Sensors Actuators A 33 (1992) 249–256.
[4] C.H. Mastrangelo, X. Zhang, W.C. Tang, Surface micromachined capacitive differential pressure sensor with lithographically-defined

silicon diaphragm, in: The Eighth International Conference on Solid-State Sensors and Actuators, Eurosensor IX Stockholm, 25–29 June 1995, pp. 612–615.
[5] H.K. Kuiken, Etching: a two-dimensional mathematical approach, Proc. R. Soc. Lond. A 392 (1984) 199–225.
[6] H.K. Kuiken, Etching through a slit, Proc. R. Soc. Lond. A 396 (1984) 95–117.
[7] C. Vuik, C. Cuvelier, Numerical solution of an etching problem, J. Comput. Phys. 59 (1985) 247–263.
[8] J.C. Bruch Jr., C.A. Papadopoulos, J.M. Sloss, Parallel computing used in solving wet chemical etching semiconductor fabrication problems, GAKUTO Int. Ser., Math. Sci. Appl. 1 (1993) 281–292.
[9] H.K. Kuiken, J.J. Kelly, P.H.L. Notten, Etching profiles at resist edges—I. Mathematical models for diffusion-controlled cases, J. Electrochem. Soc. 133 (1986) 1217–1226.
[10] P.H.L. Notten, J.J. Kelly, H.K. Kuiken, Etching profiles at resist edges—II. Experimental confirmation of models using GaAs, J. Electrochem. Soc. 133 (1986) 1226–1232.
[11] C.B. Shin, D.J. Economou, Effect of transport and reaction on the shape evolution of cavities during wet chemical etching, J. Electrochem. Soc. 136 (1989) 1997–2004.
[12] C.B. Shin, D.J. Economou, Forced and natural convection effects on the shape evolution of cavities during wet chemical etching, J. Electrochem. Soc. 138 (1991) 527–538.
[13] W.J. Li, J.C. Shih, J.D. Mai, C.-M. Ho, J. Liu, Y.-C. Tai, Numerical simulation for the sacrificial release of MEMS square diaphragms, in: 1st International Conference on MSMSSA, San Jose, USA, April 1998.
[14] K. Kaneko, T. Noda, M. Sakata, T. Uchiyama, Observation and numerical simulation for wet chemical etching process of semiconductor, in: Proceedings of 4th ASME–JSME Joint Fluids Engineering Conference, Honolulu, USA, 6–10 July 2003.
[15] D. Adalsteinsson, J.A. Sethian, A level set approach to a unified model for etching, deposition and lithography I: Algorithms and two-dimensional simulations, J. Comput. Phys. 120 (1995) 128–144.
[16] D. Adalsteinsson, J.A. Sethian, A level set approach to a unified model for etching, deposition and lithography II: Three-dimensional simulations, J. Comput. Phys. 122 (1995) 348–366.
[17] A. La Magna, G. D'Arrigo, G. Garozzo, C. Spinella, Computational analysis of etched profile evolution for the derivation of 2D dopant density maps in silicon, Mater. Sci. Eng. B 102 (1–3) (2003) 43–48.
[18] Y.C. Lam, J.C. Chai, P. Rath, H. Zheng, V.M. Murukeshan, A fixed grid method for chemical etching, Int. Commun. Heat Mass Transfer 31 (8) (2004) 1123–1131.
[19] P. Rath, J.C. Chai, H. Zheng, Y.C. Lam, V.M. Murukeshan, H. Zhu, A fixed-grid approach for diffusion- and reaction-controlled wet chemical etching, Int. J. Heat Mass Transfer 48 (2005) 2140–2149.
[20] N. Shamsundar, E.M. Sparrow, Analysis of multidimensional conduction phase change via the enthalpy method, J. Heat Transfer 97 (1975) 333–340.
[21] N. Shamsundar, E. Rooz, Numerical methods for moving boundary problems, in: W.J. Minkowycz, E.M. Sparrow, G.E. Schneider, R.H. Pletcher (Eds.), Handbook of Numerical Heat Transfer, first ed., Wiley, New York, 1988, pp. 747–786.
[22] V.R. Voller, C. Prakash, A fixed-grid numerical modelling methodology for convection–diffusion mushy region phase-change problems, Int. J. Heat Mass Transfer 30 (8) (1987) 1709–1719.
[23] A.D. Brent, V.R. Voller, K.J. Reid, Enthalpy-porosity technique for modeling convection–diffusion phase change: application to the melting of a pure metal, Numer. Heat Transfer 13 (1988) 297–318.
[24] V.R. Voller, An overview of numerical methods for solving phase change problems, in: W.J. Minkowycz, E.M. Sparrow (Eds.), Advances in Numerical Heat Transfer, vol. 1, Taylor and Francis, 1997, pp. 344–359.
[25] C.K. Chun, S.O. Park, A fixed-grid finite-difference method for phase-change problems, Numer. Heat Transfer Part B 38 (1) (2000) 59–73.
[26] W.D. Bennon, F.P. Incropera, A continuum model for momentum, heat and species transport in binary solid–liquid phase change systems—I. Model formulation, Int. J. Heat Mass Transfer 30 (10) (1987) 2161–2170.
[27] M. Bhattacharya, T. Basak, K.G. Ayappa, A fixed-grid finite element based enthalpy formulation for generalized phase-change problems: Role of superficial mushy region, Int. J. Heat Mass Transfer 45 (24) (2002) 4881–4898.
[28] J. Kaenton, E. Semma, V. Timchenko, M.El. Ganaoui, E. Leonardi, G. Davis de Vahl, Effects of anisotropy and solid/liquid thermal conductivity ratio on flow instabilities during inverted Bridgman growth, Int. J. Heat Mass Transfer 47 (14–16) (2004) 3403–3413.
[29] J. Kaenton, G. Davis de Vahl, E. Leonardi, S.S. Leong, A numerical study of anisotropy and convection during solidification, Numer. Heat Transfer Part B 41 (3–4) (2002) 309–323.
[30] S.V. Patankar, Numerical Heat Transfer and Fluid Flow, first ed., Hemisphere, New York, 1980.